# A 3-D IMAGE CHAMBER FOR THE LAR TPC ON MULTI-LAYER PRINTED CIRCUIT BOARD

P. Benetti [f], A. Bettini [e], E. Calligarich [f], F. Casagrande [e], F. Cavanna [c], P. Cennini [a], S. Centro [e], S. Cittolin [a], D. Cline [d], C. De Vecchi [e], R. Dolfini [f], A. Gigli Berzolari [f], X. Li [b], Y. Liu [d], F. Mauri [f], C. Montanari [f], G. Muratori [d], S. Otwinowski [d], A. Pepato [e], L. Periale [g], G. Piano Mortari [c], A. Piazzoli [f], P. Picchi [b], F. Pietropaolo [e], A. Rappoldi [f], G.L. Raselli [f], P. Rossi [e], J.P. Revol [a], C. Rubbia [a], D. Scannicchio [f], S. Suzuki [g], W.H. Tian [a], S. Ventura [e], M. Verdecchia[c], H. Wang [d] and M. Zhou [d]



[a] *CERN, CH-1211, Geneva 23, Switzerland*

[b] *Lab. Naz. di Frascati dell'INFN*
*Via E.Fermi 40, Frascati (Roma), Italy*

[c] *Dipartimento di Fisica e INFN, Università dell'Aquila,*
*Via Vetoio, Coppito (AQ), Italy*

[d] *Department of Physics, UCLA, Los Angeles, CA 90024, USA*

[e] *Dipartimento di Fisica e INFN, Università di Padova*
*Via Marzolo 8, Padova, Italy*

[f] *Dipartimento di Fisica e INFN, Università di Pavia*
*Via Bassi 6, Pavia, Italy*

[g] *ICGF del CNR di Torino, Corso Fiume 4, Torino, Italy*

DFPD 94EP/04

UNIVERSITÀ DEGLI STUDI DI PADOVA
**DIPARTIMENTO DI FISICA**
**"GALILEO GALILEI"**

**ISTITUTO NAZIONALE DI FISICA NUCLEARE**
**SEZIONE DI PADOVA**

**Via Marzolo, 8 - 35131 PADOVA (ITALIA)**

# A 3-D IMAGE CHAMBER FOR THE LAR TPC ON MULTI-LAYER PRINTED CIRCUIT BOARD

P. Cennini, S. Cittolin, J.P. Revol, C. Rubbia, W.H. Tian
*CERN, CH-1211, Geneva 23, Switzerland*
X. Li, P. Picchi
*Lab. Naz. di Frascati dell'INFN, via E.Fermi 40, Frascati (Roma), Italy*
F. Cavanna, G. Piano Mortari, M. Verdecchia
*Dipartimento di Fisica e INFN, Università dell'Aquila, via Vetoio, Coppito (AQ), Italy*
D. Cline, Y. Liu, G. Muratori, S. Otwinowski, H. Wang, M. Zhou
*Department of Physics, UCLA, Los Angeles, CA 90024, USA*
A. Bettini, F. Casagrande, S. Centro, C. De Vecchi, A. Pepato, F. Pietropaolo, P. Rossi, S. Ventura
*Dipartimento di Fisica e INFN, Università di Padova, via Marzolo 8, Padova, Italy*
P. Benetti, E. Calligarich, R. Dolfini, A. Gigli Berzolari, F. Mauri, C. Montanari, A. Piazzoli, A. Rappoldi, G.L. Raselli, D. Scannicchio
*Dipartimento di Fisica e INFN, Università di Pavia, via Bassi 6, Pavia, Italy*
L. Periale, S. Suzuki,
*ICGF del CNR di Torino, corso Fiume 4, Torino, Italy*

ABSTRACT

In our research and development programme for the ICARUS experiment we have developed a novel three-dimensional read-out scheme for liquefied noble gases TPC, where no charge multiplication process takes place. The design avoids completely wire grids and is based on the multi-layer circuit technique. As a consequence it is intrinsically safe and suited to be used in large and modular structures as those foreseen for ICARUS. We describe here how the electrodes structure can be simplified leading to the new design principles. We will show the results obtained with a small prototype chamber in a 100GeV μ beam.



## 1. Introduction.

The LAr TPC was first proposed in 1977 by C. Rubbia [1] with the aim to build a detector with a large sensitive mass, that is continually sensitive, self-triggering and is able to provide three dimensional images of any ionising event, as an electronic bubble chamber. A configuration of the electrodes suitable for the three dimensional read-out of the events was proposed by E. Gatti et al. [2]. Following these ideas we developed, in the framework of the ICARUS experiment, a multi-plane wire chamber made of several parallel wire grids to be used as read-out electrodes of the LAr TPC. A 3 ton prototype making use of such technology has been in operation since May 1991 [3].

The chamber works as follows. A voltage is applied to each wire plane in order to ensure the transparency of the grids to the drifting electrons (see ref. [4] for a detailed explanation of this point). The position and charge of the track elements are measured by means of the current induced on each sense wire. The drifting electrons reach and cross in sequence the following wire planes: 1. A plane of wires running in the *y* direction (*x* and *y* are the two orthogonal directions along which the wires are placed), functioning as a screening grid. 2. A plane of wires running again in the *y* direction, located below the screening grid; its function is to measure by induction the *x* co-ordinate. 3. A plane of wires running in the *x* direction located below the previous plane; its function is to measure the y co-ordinate. Since this is the last sensitive plane, the electric field is such that this plane collects the drifting electrons.

An electron drifting in the sensitive volume above the screening grid does not produce any current in the co-ordinate planes (in the case of perfect shielding). A positive induced current starts in the *x* co-ordinate plane when the electron crosses the screening grid, becomes negative when the electron crosses the co-ordinate plane and ends when the electron crosses the *y* co-ordinate plane. The charge signal from the *y* co-ordinate plane has similar behaviour, with the exception that only the positive current is present.

The originality and the performance of this novel technique, applied to wire chambers of dimension up to 2.5 $m^2$ and of 2 mm grid pitch, have been discussed in detail in a recent paper [5]; nevertheless this design presents some weak points that could be potentially dangerous if the chambers are built on a very large scale (several tens of square meters).

Mechanics:

1. Each wire has to be kept in place with respect to the others without bending; this implies very accurate absolute positioning (combs), high stress (several kilograms) to tension the wires, a complicated system to safely hold the wires on the frame and finally a thick frame robust enough to absorb the forces without appreciable distortions.
2. A possible loosening of a wire inside the chamber can kill an appreciable part of the detector.
3. The low frequency microphonic noise due to vibrations of the wires.

4. The present design makes use of a large number of wires, employs different materials for the construction of the frame and is based on a mechanical structure. All this makes the chamber very delicate to handle especially during the cool-down and filling phases. Moreover the modular structure required for a very large detector makes it difficult to avoid dead spaces due to the wide frames necessary to maintain the mechanical strengthening of the wires.

Electronics:

1. The large electric fields (of the order of several kV/cm) required to ensure the correct path of the drifting electrons through the grids without unwanted losses give a supplementary stress to the wires due to electrostatic forces.
2. The chambers have to support the connections to the front-end electronics (through high voltage decoupling capacitors). This is a delicate point because several connectors are needed between the crimping pin and the preamplifier board and each of them increases the probability of electrical interruption.

Analysis:

1. The induction signals are fast (both rise and fall times last about few μs), resulting in few points on the sampled output; hence the filtering algorithms needed to enhance the signal to noise ratio are not very efficient.
2. For the same reason the only physical parameter that can be reliably extracted from the induction signals is the arrival time, usable for tracking in one plane projection. All the other relevant parameters (charge, rise time, arrival time in the orthogonal plane projection) have to be extracted from the collection signals.

The aim of this paper is to present an alternative solution for building large size 3-D image chambers with an intrinsically simpler and safer structure but with performance comparable to that of the technique previously described.

**2. The new image chamber.**

To understand the new structure of the image chamber let us start from the following configuration of the wire planes read-out electrodes:

1. a screening grid, made of parallel wires (100 μm in diameter) with a 3 mm pitch;
2. a collection plane, located 3 mm below the screen, also made of parallel wires (100 μm in diameter) and oriented in the same direction as those of the grid; their functions are alternatively of field shaping wires and of sense wires, where the drifting electrons are collected; the distance between two collection wires is 3 mm;
3. a conductive plane at a distance of 0.5 mm.



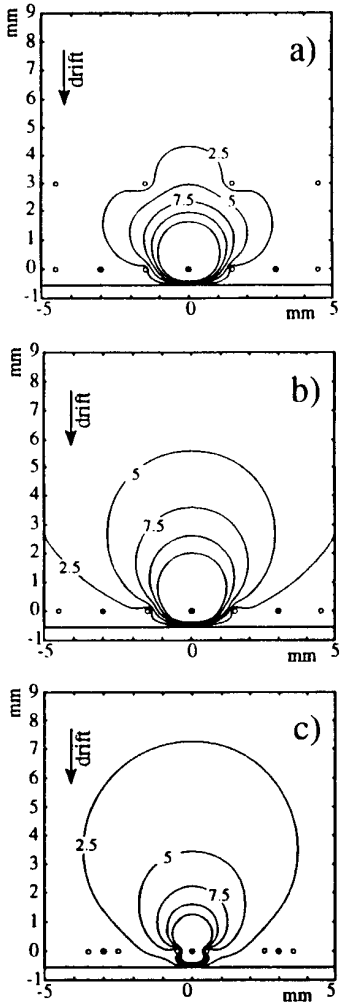


Fig.1. Equi-induction curves for the collection electrodes in the plane normal to the collection electrodes and parallel to the drift field for the three structures described in the text a) Wire chamber with screen grid. b) Chamber without screen grid. c) Chamber without grid with a different electrodes configuration.

Fig. 1a shows the map of the equi-induction contours calculated for the structure described above; the shape of these lines depends only on the geometry of the electrodes. The figure is read in the following way: a point charge placed anywhere in the space induces a fraction of its charge on the electrode (sense wire) under examination equal to the value of the contour line passing through the charge position (the percentage of induced charge is used to label the curves). One can see that, as desired, the induction is appreciable only close to the wire; the screening grid helps by "pushing" the line below its plane: this is in fact its shielding contribution.

We now proceed to simplify the electrode structure. The first step consists in eliminating the screening grid. The equi-induction curves are presented in fig. 1b. A comparison with the previous configuration shows that, as expected, the lines corresponding to the same induction now spread further away in the drift space. Notice that, on the other hand, the residual but effective shielding function is now performed by the screening wires that are co-planar with the sense wires and by the conductive plane.

The shielding action can be improved by positioning the screening wires closer to the sense ones. We consider a configuration with two screening wires at the sides of each sense wire at a distance of 0.5 mm. The calculated equi-induction map is shown in fig. 1c. In this new configuration the curves are nearer to the sense wires, similar to those of fig. 1a, for which the grid was present.

We next discuss how to use the "non-gridded" configuration for a 3-D imaging read-out. The wire plane represented in fig.1b or 1c can be used as the collection plane by giving a suitable potential difference between field and sense wires, to focus the field lines on the collection wires. In

practice we polarize the sense wires at +300 V and the field wires at -300 V, in order to keep the average potential of the collection plane at ground. To measure the second co-ordinate we must have an induction electrode plane.

In the configuration of Gatti et al. the induction plane was placed in front of the collection one and the voltage applied was such that this grid was completely transparent to the drifting electrons. In this scheme the drifting electrons, moving across this plane, give by induction the signal to be detected; they then move toward the second plane where they are collected.

In the new configuration we substitute the conductive plane behind the collection grid with a plane made of parallel electrodes acting as the induction plane. In fact the induction signal due to electrons moving above the collection plane is visible even below the collection plane because the latter does not act as a perfect screen. The problem is to try to maximise this induction signal without deteriorating the collection one. The simplest way consists in increasing the width of the induction electrodes while minimising that of the collection electrodes, in order to favour the charge induced on the induction plane due to the solid angle effect, and in working with a small gap between the two planes.

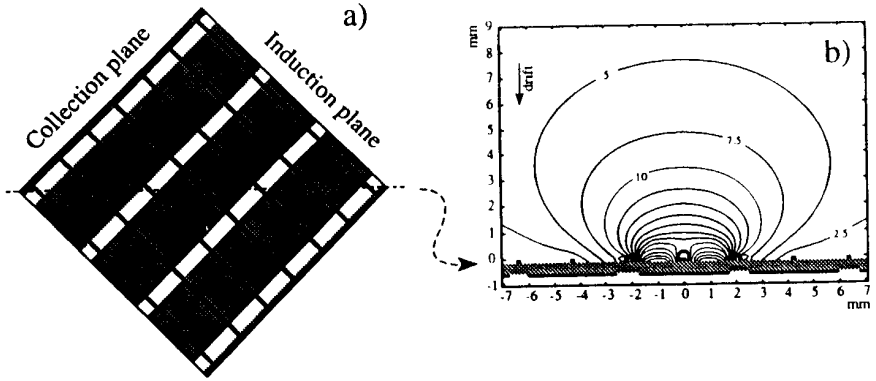


Fig.2. Equi-induction curves for the induction electrodes for the configuration described in the text. The map in b) is shown in a plane containing the drift field and at 45° with both collection and induction electrodes.

The equi-induction map for the induction electrodes is shown in fig. 2 for a configuration consisting of a collection plane as that of fig.1b and an induction plane located 0.5 mm below it made of sense strips 2.54 mm wide with a 3 mm pitch, perpendicular to the collection electrodes. The map is in a plane perpendicular to the read-out electrodes crossing them at 45° and refers to the central induction strip.

We are now ready for the second and last step in the simplification process. A very important feature of the new configuration is that the drifting electrodes never cross any grid. As a consequence, the structure can be realised with metal strips deposited on the two faces of a dielectric support employing, in practice, printed circuit techniques.

We have constructed a read-out structure consisting of a 0.5 mm thick vetronite sheet with the collection strips on the upper face and the induction strips on the lower one. The structure is kept rigid with a second vetronite sheet, 2 mm thick, glued on the lower side. Collection and induction strips are mutually perpendicular and have both a 3 mm pitch. The collection strips are 0.1 mm wide, while the induction ones are 2.54 mm wide. Two field strips (0.1 mm wide) are located at the two sides of each collection strip, on the same plane and at distance of 0.5 mm.

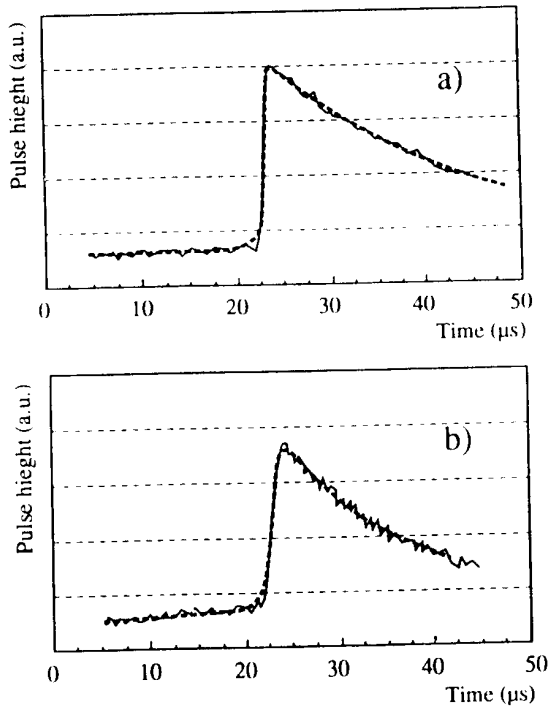


Fig.3. Measured and calculated shapes for the "collection" signals for a) the gridded configuration and b) the ungridded configuration.

We now discuss the collection and induction signal shapes in this new configuration. First we calculate the time dependence of the signal induced on the sense wire by moving the charge of a track segment along trajectories parallel to the drift field with appropriate velocities. We will consider tracks parallel to the read-out planes. Fig. 3a shows the result of our calculation for

the "gridded" configuration of fig.1a. For comparison we also show, superimposed, an experimental signal collected with a small LAr TPC exposed to a μ beam (see section 3). The excellent agreement denotes the reliability of our calculation.

The signal shape (theoretical and experimental) for the "ungridded" configuration of fig. 1b is shown in fig. 3b; the main difference with the shape of fig. 3a is in the long leading tail which is due to the shielding inefficiency. Nevertheless the main physical parameters (pulse height, arrival time, signal slope) can be extracted with equal reliability from the collection signal shapes in both configurations described above.

The calculated induction signal shape, superimposed on a real pulse, for the ungridded configuration of fig.1b, is shown in fig. 4. Note that the induction signal now has a shape, and height, very similar to that of the collection one (but of opposite polarity); this could lead to a more reliable extraction of the physical parameters also for the induction case.

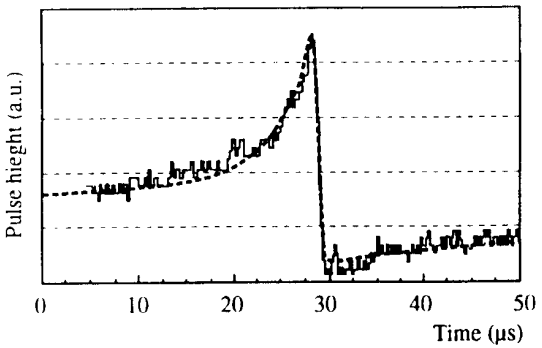


Fig.4. Measured and calculated shapes for the "induction" signal for the ungridded configuration.

We stress here that, from a practical point of view, a very important feature of this new configuration is that a chamber can be constructed on a printed circuit board. The fact of having eliminated all the wires makes the structure intrinsically safer and stable. Another advantage is that the voltage difference applied on the collection electrodes is now very small (a few hundreds of volts); this leads to a more uniform electric field in the drift volume and the use of smaller and safer decoupling capacitors. As a consequence the front-end electronics can be located very near to the chamber, even inside the LAr, thus avoiding long cables that increase the input capacitance (and hence the series noise) and the microphonic pick-up. Notice also that, as a by-product, the connections of the sense electrodes to the front-end electronics and the high-voltage distribution can be realised as an integrated part of this printed circuit board (making use of the multi-layer technique).

A possible drawback of this solution is the increase of the detector capacitance due to two factors: the reduction of the inter-plane gap (in our case from 3 mm to 0.5 mm) and the higher



dielectric constant of the printed circuit support with respect to that of the argon ($\varepsilon_r$ = 1.5). This could worsen the S/N and therefore degrade the detector performance. A way to partially avoid this problem consists in using a support with low dielectric constant (e.g. Teflon, $\varepsilon_r$ = 2.2) and to divide each strip into segments of the order of a few metres, each of which is read by one pre-amplifier whose output is then "ORed" with that of the other segments. A realistic value of the achievable specific capacitance is about 20-30 pF/m, not different from that of the wire chamber.

**3. Experimental results.**

To compare with real data the performance of the two configurations described in the previous sections, we built two small 3-D image chambers, one using the wire technique, the other the printed board technique. The wire chamber consisted of a sequence of three wire planes: the grid (100 μm diameter wires at 3 mm pitch), the induction plane (100 μm diameter wires at 3 mm pitch, sense and field wires interleaved), the collection plane (same geometry of the induction plane, with wires perpendicular to the induction ones). The distance between two contiguous planes was 3 mm. The second chamber had the configuration shown in fig. 1b and fig. 2. In both cases the number of sense wires was 19 induction and 19 collection. These chambers were used in turn as read-out electrodes of a LAr TPC whose drift length was 13 cm. We exposed the TPC to the CERN-SPS 100 GeV μ beam.

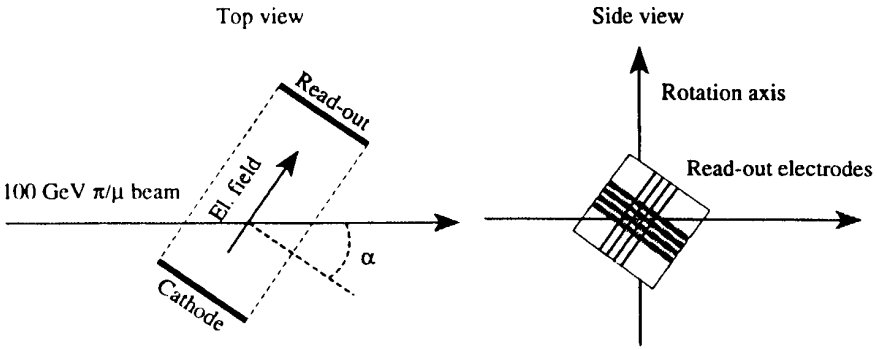


Fig.5. Schematics of the TPC layout in the beam.

The TPC was placed with the drifting electric field parallel to the floor and with the possibility of rotating it around a vertical axis (see fig. 5). The wire chamber was placed with the collection wires vertical, in order to see the signal due to the ionising beam on all the collection wires. Unfortunately only one induction wire was hit in each event.

In the printed board case, instead, a rotation of 36° around the drift axis was given to the board in such a way that a track image, made of several contiguous wire hits, was visible on both the collection and induction planes; the image of a multi-track event can be seen in fig. 6. We measured the detector response to minimum ionising particles (m.i.p.), in terms of energy and spatial resolution, as a function of the electric field strength and of the angle between the track and the drift direction.

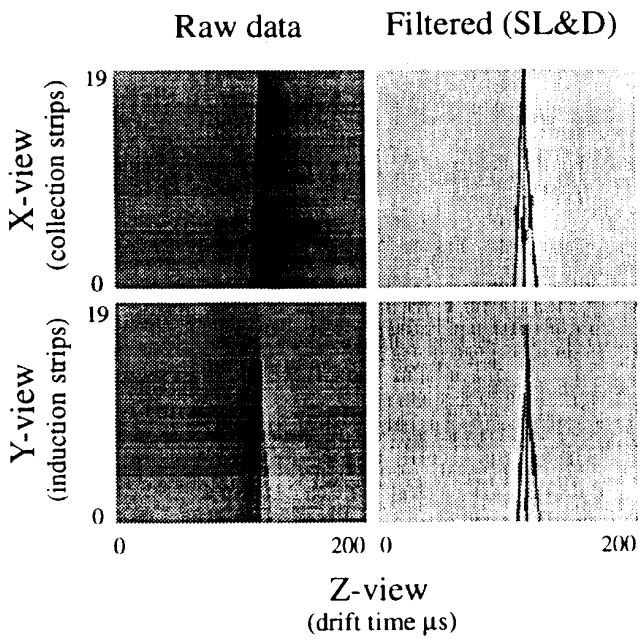


Fig.6. The two orthogonal views (rough and filtered data) of a three-prong interaction from the multi-layer chamber.

3.1 Electron lifetime.

A first important result is that no appreciable difference in the electron lifetime has been noticed (it was always higher than 3 ms) in the two cases. This confirms [6] that at LAr temperatures the outgassing of electronegative impurities from any material employed in the construction of the TPC is negligible.

3.2 Energy resolution.

The energy resolution can be extracted from the distribution of the charge deposited by minimum ionising particles on single sense strips by fitting with the convolution of a Landau and a Gaussian functions. This is possible because the relation between the energy deposited and the charge collected, dominated by the electron-ion recombination, for minimum ionising particles is linear around the Landau peak. The Landau parameter is related to the intrinsic fluctuation of $dE/dx$ in LAr, while the variance of the Gaussian takes into account the contribution of the electronic noise, calibration and the signal extraction algorithm.

The results obtained with both read-out chambers are very similar: the Landau parameter is around 800 electrons, in agreement with the value predicted by the Vavilov model [7]; the overall Gaussian noise is about 400 electrons in agreement with the measurement done on the width of the test pulse height distribution. In fig. 7 we present the two distributions of the charge deposited on the collection electrodes obtained with the multi-layer chamber and with the wire chamber. The data are relative to tracks running parallel to the chamber plane and a drift field of 500 V/cm. The good agreement is evident.

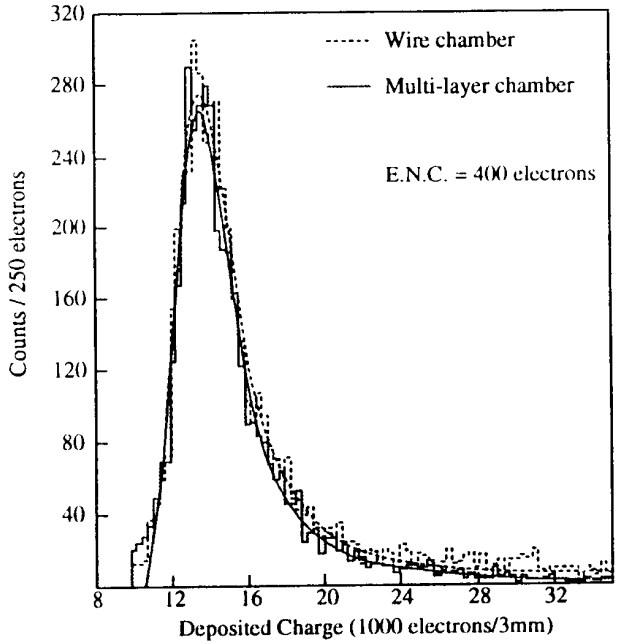


Fig.7. Collected charge distributions on 3mm length for beam tracks crossing the chamber parallel to the electrode plane for wire chamber and multilayer chamber.

3.3 Electric field and angular dependence of the free electron yield.

The peak of the charge distributions can be used to measure the electric field dependence of the charge released by a m.i.p. over 3 mm and, as a consequence, the electron-ion recombination effect. Moreover the data taken on the beam can be used to measure the dependence of the collected charge as a function of the angle ($\alpha$ in Fig.5) between the electric field lines and the track direction. Angle dependent effects could be induced by the lack of a screening grid in the multi-layer chamber. Such a dependence could worsen the overall energy resolution mainly for low energy tracks (e.g.: few MeV electrons) for which multiple scattering makes the track direction vary considerably even within a single wire pitch.

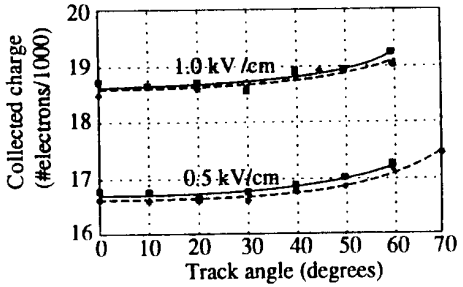


Fig.8. Angular dependence of the (peak) collected charge for both the wire chamber (grey dots and dotted lines) and the multi-layer chamber (black squares and continuous line) at two different drift fields.

The experimental data are presented in fig. 8: the peak of charge distribution at each angle normalised to the wire pitch (3 mm) is plotted against the track angle for two electric field strengths (500 V/cm and 1 kV/cm) for the both read-out chambers. The slight increase visible at large angles is due to the change of the effective track sampling pitch (3 mm at 0°, 6 mm at 60° and 9 mm at 70°) which in turn introduces a well known peak shift in the normalised Landau distribution. This is confirmed by the analysis performed on Montecarlo data.
The agreement between the two chambers is fully satisfactory both for the electric field dependence and the angular behaviour.

3.4 Spatial resolution.

The single point spatial resolution along the drift direction can be evaluated by fitting event by event the arrival times versus the wire positions with a straight line and then plotting the distribution of the residuals to the fit. The width of the distribution gives the arrival time resolution. The best result is obtained if the straight line fit is made on three contigous wires at the time to minimise the contribution of the multiple scattering. Knowing the electron drift velocity it is straightforward to obtain the single point spatial resolution. In fig. 9 we show



both the resolution on the drift time measurement and the spatial resolution (obtained from the latter dividing by the drift velocity) versus the electric field. Time resolution worsen at lower fields due to the diffusion of the charge drifting for longer times; on the other hand, space resolution becomes better because the decrease of the drift velocity overcompensate the effect of the broadening of the signal. For the present discussion it is important to notice that for both the read-out chambers no appreciable difference was measured.

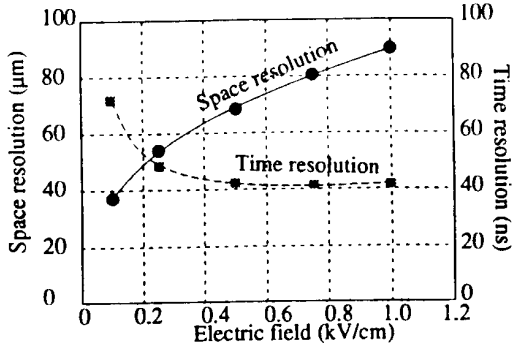


Fig.9. Resolution in the drift time measurement (right scale) and space resolution in the drift co-ordinate measurement (left scale) as functions of the drift field.

## 4. Conclusion

We have developed a new 3-D imaging read-out structure suitable to be employed in any liquefied noble gas TPC where no charge multiplication process occurs. The design, based on the multi-layer printed circuit board technique, is intrinsically safe, both mechanically and electrically, and is suited to be built in large size and modular structures, such as those foreseen for the ICARUS experiment at Gran Sasso. Moreover the scheme allows one to vary the pitch of the segmented electrodes within the same detector. This feature is particularly appropriate for the ICARUS experiment because it enhances its intrinsic characteristic of being a multipurpose detector.

## 5. References

[1] C.Rubbia, CERN-EP Internal Report 77-8 (1977).
[2] E.Gatti et al., IEEE Trans. Nucl. Sci. NS-26 (1979) 2910.
[3] P.Benetti et al., Nucl. Instr. and Meth. A322 (1993) 395.
[4] O.Bunemann et al. Can. J. of Res. 27 (1947) 191.
[5] P.Benetti et al. submitted to Nucl. Instr. and Meth.
[6] A. Bettini et al., Nucl. Instr. and Meth. A305 (1991) 177.
[7] P.V.Vavilov, Soviet Physics JETP 5 (1957) 749.